Available online at www.sciencedirect.com
SCIENCE DIRECT®
Journal of Nuclear Materials 319 (2003) 44–50
journal of nuclear materials
www.elsevier.com/locate/jnucmat

Design and fabrication of specific ceramic–metallic fuels and targets

A. Fernández *, R.J.M. Konings, J. Somers

European Commission, Joint Research Centre, Institute for Transuranium Elements, P.O. Box 2340, D-76125 Karlsruhe, Germany

Abstract

The fabrication of ceramic–metallic (cermet) composite fuel, containing $(Y,An,Zr)O_{2-x}$ spheres, by dust free processes has been studied. The influence of several process parameters, such as, ceramic volume fraction, compaction pressure and sintering temperature, on the microstructure of the final composite have been investigated and optimised using cerium as a stand for americium and two metal matrices namely molybdenum and stainless steel. In addition, a cermet fuel with (near) spherical $(Y,Pu,Zr)O_{2-x}$ particles, dispersed in stainless steel matrix, has been successfully fabricated and characterized.

1. Introduction

New concepts are required for the design and fabrication of targets and fuels for the transmutation of actinides. Different suggestions have been made in recent years, mainly depending on fuel cycle strategy considerations. Two general approaches can be distinguished: (a) the mixing of small quantities of the minor actinides (up to about 2.5 wt%) together with plutonium in the fuels of standard reactor cores, and (b) the use of dedicated fuels/targets, which have a higher content of plutonium and minor actinides (typically 20 wt%), in dedicated actinide 'burners'. The number of subassemblies required for the same minor actinide mass throughput is smaller in the latter option, which has the advantage that conventional production facilities can still be used to produce driver fuels, in parallel to specific minor actinide fabrication installations for the targets.

It is obvious that when a fuel or target does not contain ^{238}U, the transmutation efficiency is higher. Since the transmutation process is essentially based on fissioning of actinides, a high burn-up of the fuel/target is required to reach high efficiency. This will lead to high demands on the performance of the fuel in view of the concomitant high fission-gas and helium production, fuel swelling and chemical and mechanical fuel cladding interaction. All of these will exceed the levels known in existing fast reactor fuels. Dispersions of actinide oxides in a ceramic (cercer) or metallic (cermet) uranium-free matrix are presently considered as targets for the transmutation of americium [1,2]. The main advantages of such composite targets compared to a solid solution is that it potentially (this should be examined after long-term irradiation programs) minimizes irradiation-induced property changes in the fuel pellets by localizing the fission damage in a limited geometric domain within the fuel. The cermet fuel offers further advantages such as, its ability to retain fission gases, volatile fission products and helium in the fuel, and its high thermal conductivity, which either permits higher actinide loading or lower operating temperatures. Previous investigations have shown that, if the proportion of the fissile ceramic phase does not exceed 60% of the volume of the pellet, the thermal conductivity of the composite is still closer to that of a metal than that of a ceramic [3].

From their neutronic aspects, the most interesting metal matrices for cermet fuels are steel, vanadium, molybdenum, chromium for fast systems and zirconium or Zircaloy for thermal reactors. The neutron-capture

* Corresponding author. Tel.: +49-7247 951 246; fax: +49-7247 951 99246.
E-mail address: fernandez@itu.fzk.de (A. Fernández).

0022-3115/03/$ - see front matter © 2003 Elsevier Science B.V. All rights reserved.
doi:10.1016/S0022-3115(03)00132-6

cross-sections of some of these metals are not insignificant, however, and their activation during irradiation needs to be analysed in more detail. For example, neutron activation of natural Mo will lead to the formation of technetium, which increases the long-term toxicity as a long-lived waste is produced. The use of molybdenum depleted in the high neutron absorption cross-section isotope ^{95}Mo is technically feasible and thus would help to overcome this problem [4].

The fabrication of composite pellets is considerably more difficult than solid solution oxide pellets. This is a result of the specific requirements of size and distribution of the dispersed actinide phase. The major problem to be solved is the control of the distribution of ceramic phase in the ductile metal matrix. As is the case for cercer materials, spherical particles are ideal and stabilisation of the actinide (Pu, Np or Am) in a host phase (e.g. stabilised zirconia) is also preferred [1]. The fabrication of cermet fuel generally needs a powder metallurgy step, where the metal powder is mixed with the ceramic phase, pressed into pellets, preferably by cold compaction and sintered at high temperature. The existing literature information on the fabrication of cermet fuels is limited to uranium oxide as actinide phase or inactive elements such as Ce or Nd to simulate the actinides. In the 1960s cermet fabrication was performed in the USA where UO_2 was dispersed in iron, niobium, aluminium, zirconium and alloys e.g. austenitic or ferritic stainless steel, or Zircaloy. When working with ductile metals that are not very sensitive to oxygen (e.g. Mo), the fabrication is relatively simple and can be based on powder mixing without undue precautions. For zirconium, however, this is not the case, and more complex fabrication techniques have been investigated [5–7].

In this investigation, a systematic study of the fabrication process was made to obtain high-density cermet pellets containing ceria doped YSZ dispersed in molybdenum or stainless steel. This paper describes the results of fabrication tests and the microstructural characterization of these cermet compounds. The fabrication results of $(Y,Pu,Zr)O_{2-x}$ dispersed in stainless steel for an irradiation experiment in the HFR-Petten reactor are also presented.

2. Experimental procedure

2.1. Sample preparation

The fabrication of ceramic–metal (cermet) composite pellets of $(Y,An,Zr)O_{2-x}$–Me (Me = molybdenum, or stainless steel) pellets is based on the fabrication of particles containing the actinide phase by a combination of the external gelation, gel supported precipitation [8,9], and the infiltration methods [10], followed by mixing of the particles and the matrix powder by conventional blending methods (see Fig. 1). The effect of important parameters related to composite pellets fabrication, such as, the volume fraction of ceramic (actinide phase) and the size of the ceramic particles, have been investigated. The process has been tested and validated with cerium and plutonium at the laboratory scale and the main results are described here. The actual fabrication of americium and eventually curium-containing materials will be performed in a set of specially constructed shielded cells, which are under construction at present [11].

In a first step highly porous spheres of yttria-stabilised zirconium oxide $Y_{0.17}Zr_{0.83}O_{1.92}$, YSZ, are produced by the external gelation method, which guarantees a solid solution as the final product [12]. The YSZ spheres produced in this way have a polydisperse size distribution in the 40 and 150 μm range, and a specific surface area of 67.2 $m^2\,g^{-1}$. X-ray diffraction studies of sintered spheres indicated a cubic crystal structure with a measured lattice parameter of 0.5140 ± 0.0003 nm, which is

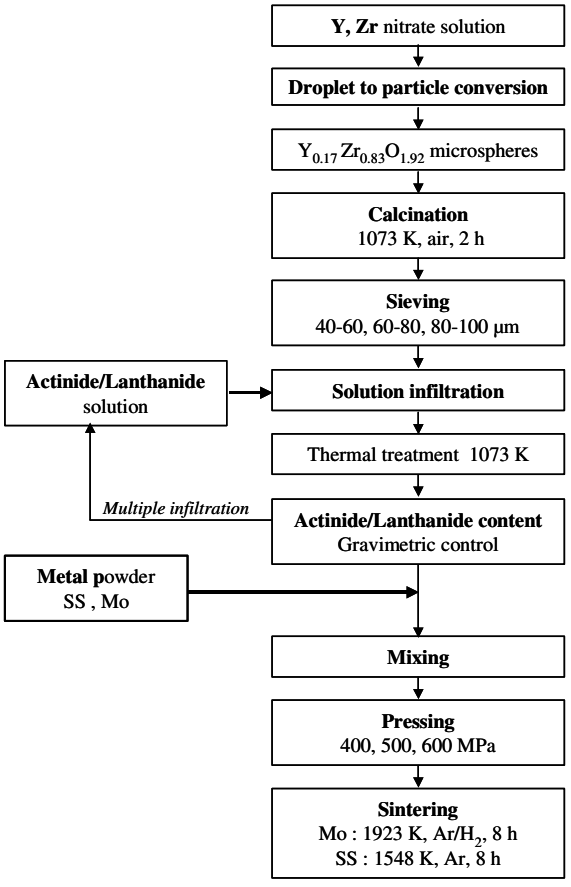

Fig. 1. Schematic flow chart of the cermet fabrication process.

in agreement with the published values for $Y_{0.15}Zr_{0.85}O_{1.93}$ [13].

After their calcination at 1073 K in air the YSZ spheres were sieved and specific size fractions (40–60, 60–80 and 80–100 μm) were selected. Each size fraction was infiltrated with a cerium nitrate solution (300 $g\,l^{-1}$) to reach the required metal content. The 60–80 size fraction was also infiltrated with a plutonium nitrate solution (216 $g\,l^{-1}$). To reach sufficiently high Ce and Pu concentration the infiltration step was repeated following an intermediate thermal treatment at 1073 K for 2 h in air to evaporate excess of water and convert the infiltrated nitrate phase to the corresponding oxide. The metal content was determined by gravimetric analysis of the spheres before infiltration and after the calcination step. The final compositions of the lanthanide and actinide doped YSZ beads after calcination are listed in Table 1. In the composite fuel types, the $(Y,Ce,Zr)O_{2-x}$, and $(Y,Pu,Zr)O_{2-x}$ phase were mixed with molybdenum (FLUKA; purity 99.7%, particle size 45 μm) and stainless steel (ALFA AESAR, SS 316L type with the weight composition: Fe 67.5%, Cr 17%, Ni 13%, Mo 2.5%, and particle size: 45 μm) powders that act as matrix for the actinide doped spheres.

Pressing tests on both commercial molybdenum and stainless steel powders without inclusion of YSZ spheres gave densities after sintering in argon of $92.1 \pm 0.8\%$ and $93.6 \pm 0.2\%$ of the theoretical density (TD), respectively. For the fabrication of cermet composites the metal powders were mixed with the infiltrated YSZ spheres and compacted into pellets with a biaxial press at 400, 500 and 600 MPa, following addition of zinc stearate as lubricant. Sintering was performed at 1923 K for 8 h in Ar/H_2 for pellets with molybdenum and at 1548 K for 3 h in argon for pellets with stainless steel.

2.2. Image analysis

The microstructure of the polished surfaces of sectioned pellets was investigated by optical microscopy. Each sample was divided in eight fields and micrographs were taken in each of them. All micrographs covered an identical area, had the same resolution (number of pixels), and scale. Subsequently, they were analysed using WIN software from Leica [14]. The number of beads and their area were evaluated from the image in each field. The standard deviation in area, σ_A, can be calculated from

$$\sigma_A^2 = \frac{\sum_{i=1}^{n}(A_i - \bar{A})^2}{n-1}, \tag{1}$$

where $n = 8$ is the number of fields analysed, A_i the area occupied by the sectioned ceramic particles and $\bar{A}$ the average area occupied by the sectioned particles in all fields analysed. A similar evaluation can be made on the basis of the number of particles. The homogeneity distribution (HD) is calculated from [15]

$$\mathrm{HD} = \frac{\sigma_A}{\bar{A}}. \tag{2}$$

Small HD values indicate a higher level of microstructural homogeneity, with $\mathrm{HD} = 0$ being the ideal case, while $\mathrm{HD} \geqslant 20$ is unacceptable [16]. In this paper, HD was evaluated from particle area measurements. It is noted that by analysing two-dimensional cross-sections of three-dimensional microstructures some information is inevitably lost. No dimensional corrections were applied to account for this effect.

3. Results and discussion

3.1. Effect of the ceramic particles size and sintering conditions on densification

Three different size fractions of $Y_{0.129}Ce_{0.234}Zr_{0.637}O_{2-x}$ have been used to fabricate cermet pellets with molybdenum and stainless steel. The infiltrated beads were mixed with the required amount of metal powder to reach a dilution factor of 20% in volume. After addition of lubricant (zinc stearate), they were compacted into pellets and sintered under the appropriate conditions (temperature and atmosphere), as shown in Table 2. The final densities of the pellets are shown in Table 3. Densities higher than 90% of the TD were obtained for pellets with Mo as matrix, while for SS pellets the final density was between 81% and 83% TD. The latter low densities are due to the lower temperature reached during the sintering step (only 1548 K)

Table 1
Ceria doped – YSZ compounds fabricated by infiltration

YSZ size/μm	Fraction MeO_2[a]/wt%	Composition
40–60	31.2	$Y_{0.129}Ce_{0.234}Zr_{0.637}O_{2-x}$
60–80	31.2	
80–100	31.2	
60–80	41.4	$Y_{0.128}Pu_{0.241}Zr_{0.631}O_{2-x}$

[a] Me = Ce and Pu.

Table 2
Fabrication parameters for cermets with Mo and SS as matrix

	Mo	SS 316L	
Compaction pressure/MPa	400	400	400
Ceramic beads			
Thermal pre-treatment/K	1073	1073	1423
Beads fraction/vol.%	20	20	20
Sintering			
Temperature/K	1923	1548	1548
Time/h	8	3	3
Atmosphere	Ar/H_2	Ar	Ar

Table 3
Effect of size of the ceramic beads on the final density

YSZ beads size (μm)	Samples		
	Mo	SS 316L	
	1073 K Sintered density (% TD)	1073 K Sintered density (% TD)	1423 K Sintered density (% TD)
40–60	92.2 ± 0.4	81.0 ± 0.3	92.1 ± 0.3
60–80	91.1 ± 0.3	83.1 ± 0.4	93.1 ± 0.6
80–100	90.7 ± 0.3	81.2 ± 0.5	93.7 ± 0.1

Cermets with Mo and SS as matrix. Ceramic volume fraction 20%.

as the melting point of SS 316L is 1663 K. At this temperature the ceramic beads were themselves not sintered. To avoid this problem a second batch was made, where the beads were thermally treated at 1423 K in air for 4 h to sinter the beads (at least partially). Higher temperatures would have been preferable but were not possible as the beads tend to form hard agglomerates, which are totally unsuited for the fabrication of composites. After this thermal treatment the beads were mixed, pressed and sintered in the same way as before, and steel cermet pellets with a final density above 92% TD were produced. For Mo pellets, the smaller size fraction gave slightly higher density, but for SS pellets the effect was opposite. In both cases, independently of the ceramic bead size, the final density is between 90% and 94% TD (i.e. porosity is between 10% and 6%). This porosity has a beneficial effect in minimizing the swelling during irradiation of composite fuel types, as has been observed for stainless steel–UO_2 dispersions [17], where 98% TD dense pellets exhibited volume changes up to 1–25% but those with 90–95% TD showed no volume change even at higher burn-ups.

Ceramographic examinations and image analysis were performed on a pellet from each batch. In all cases the micrographs shown an intimate and complete contact between the beads and the metallic matrix which guarantees maximum thermal benefit of the metal matrix and minimizes the temperature in the oxide beads. As an example micrographs at different magnifications of the stainless steel cermet pellet with a ceramic particle size of 60–80 μm are given in Fig. 2. The HD values calculated from image analysis are given in Table 4. For each batch the HD values are very low (HD = 4–5), which indicates an even distribution of the beads within the pellet. In a similar investigation on $(Y,Ce,Zr)O_{2-x}$–MgO cercer pellets, produced by the same fabrication method and with the same type of particles, image analysis gave higher HD values (HD from 6 to 11) [18].

3.2. Effect of volume fraction of the ceramic phase

The problems that arise in fabrication of cermet composites are generally associated with the incorporation of a brittle material (ceramic phase) into a ductile matrix. The ease of fabrication therefore depends critically on the volume of ceramic phase and its distribution. The volume of the dispersed phase of a suitable particle size that can be accommodated in a metal or other matrix depends largely on the shape and size of the particle. A systematic study has been performed to determine the maximum volume of ceramic phase that can be incorporated into a metallic matrix, while still meeting specifications (density, homogeneity) required for reactor irradiation. For this purpose, cermets with four

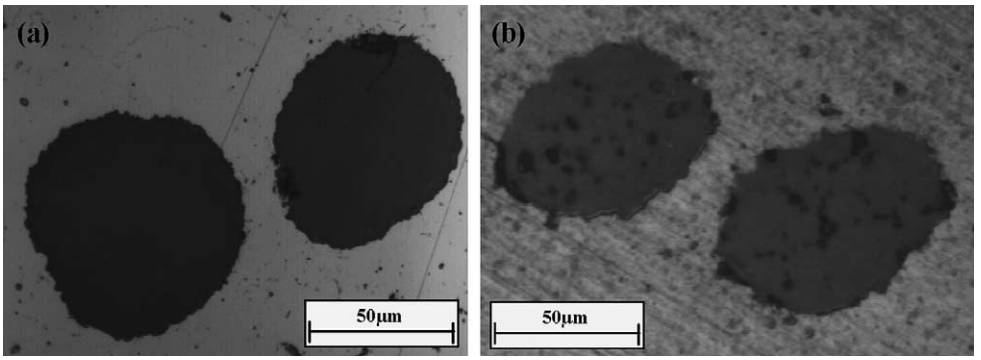

Fig. 2. Optical micrographs of a stainless steel (a) and a molybdenum (b) cermet pellet with a ceramic particle size of 60–80 μm. Ceramic beads fraction 20% in volume.

Table 4
HD values for molybdenum and stainless steel cermet pellets as a function of the particle size and the ceramic volume fraction

	Ceramic phase $(Y,Ce,Zr)O_{2-x}$	
	Mo	SS 316L
Particle size/μm		
40–60	4.2 ± 0.3	4.0 ± 0.3
60–80	4.4 ± 0.3	4.3 ± 0.3
80–100	5.0 ± 0.3	5.3 ± 0.3
Beads fraction/vol.%		
10	4.7 ± 0.3	5.6 ± 0.3
20	5.9 ± 0.3	4.7 ± 0.3
40	6.0 ± 0.3	6.2 ± 0.3
60	–	–

different ceramic fractions, i.e. 10%, 20%, 40% and 60% in volume have been fabricated. The size of the calcined YSZ beads was 60–80 μm. They were pre-sintered at 1423 K in air before mixing with the metal powder. Fig. 3 shows the effect of volume fraction of ceria doped YSZ on the final density of $(Y,Ce,Zr)O_{2-x}$–SS cermet. The density decreased dramatically with increasing $(Y,Ce,Zr)O_{2-x}$ content. This effect was expected and it is due to the low sintering temperature (1548 K), which is not enough to complete the densification of the ceramic phase. Fig. 4 shows the effect of volume fraction of the ceria doped YSZ on the final density of $(Y,Ce,Zr)O_{2-x}$–Mo cermet. In this case the higher sintering temperature (1923 K) permits the complete densification of both phases and densities above 90% TD were obtained for all compositions.

One pellet from each dilution ratio of the ceramic phase was axially sectioned, polished and micrographs were taken. For all cases, simple visual inspection indicates that all particles are uniformly distributed in the matrix. This is corroborated by the image analysis and

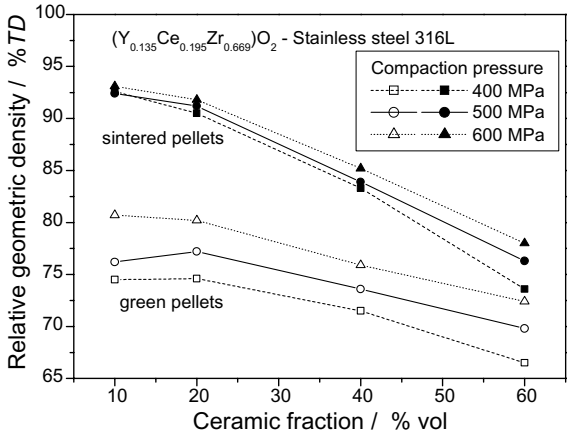

Fig. 3. Relative geometric density of stainless steel cermet pellets with different ceramic volume fractions as a function of the compaction pressure.

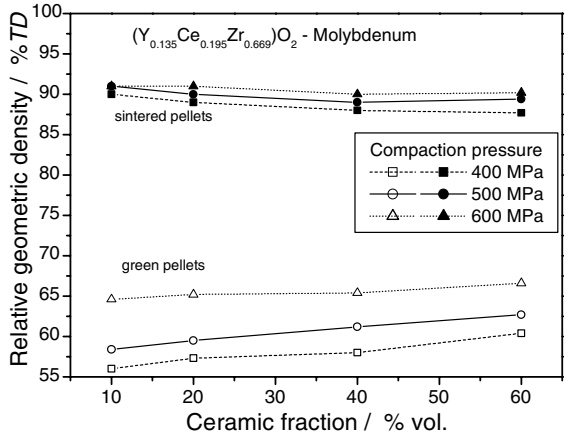

Fig. 4. Relative geometric density of molybdenum cermet pellets with different ceramic volume fractions as a function of the compaction pressure.

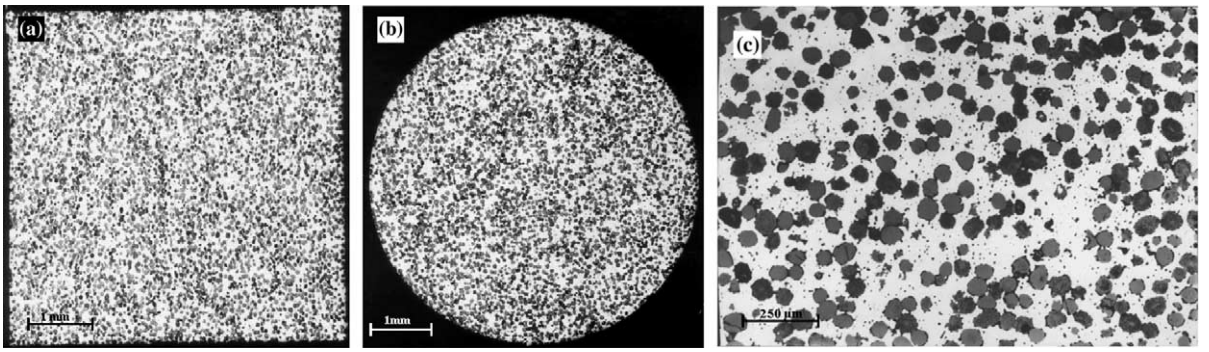

Fig. 5. α-autoradiographs of an axial (a) and a radial (b) section and optical micrograph (c) of an axial section of a $Y_{0.128}Pu_{0.241}Zr_{0.631}O_{2-x}$–SS pellet. HD = 4.1 ± 0.2.

the small HD value determined (see Table 4). For pellets with 60 vol.% of ceramic phase, however, it was not possible to perform the image analysis due to the high content of beads and their interconnection with small cracks.

Although fabrication of cermet pellets with 60 vol.% of ceramic phase (fuel-bearing phase) have been demonstrated, the main advantage (apart from the thermal conductivity) of the dispersed type fuel is the localization the fission damage in a reduced domain within the fuel. Obviously, the larger the fraction of ceramic phase the smaller the average interparticle distance which leads to an increase in the volume of damaged matrix. This effect has been observed in cermets with a large volume fraction of the fuel-bearing phase in an irradiation experiment, where the fuel contained 50 vol.% of large uranium metal particles surrounded by magnesium or magnesium–silicon alloy [19]. Due to the small interparticle distance a complete loss of ductility was observed following irradiation to 0.1% burn-up of the uranium atoms.

3.3. Fabrication of $Y_{0.128}Pu_{0.241}Zr_{0.631}O_{2-x}$–stainless steel pellets

A cermet fuel with a Pu density of 0.9 $g\,cm^{-3}$ (stainless steel based cermet pellets containing 38.5% in volume of spherical ($Y_{0.128}Pu_{0.241}Zr_{0.631}O_{2-x}$ beads) has been fabricated and characterized for an irradiation experiment in the HFR-Petten reactor. This irradiation experiment will compare the performance of this cermet fuel with an homogeneous $(Y,Pu,Zr)O_{2-x}$ fuel in a tailored fast neutron spectrum. The size of the ceramic fuel-bearing particles before pre-sintering was between 60 and 80 μm. The cermet pellets were fabricated following the process described above, but the beads were pre-sintered at 1423 K in argon instead of air. After sintering under argon, the pellet diameters were 5.41 ± 0.10 mm, their height 7.5 ± 0.1 mm and their density 87.2 ± 0.2% TD. Again this slightly lower pellet density is mainly due to the incomplete densification of the plutonium containing particles, as has been discussed above for the studies using cerium. Previous irradiation experience with stainless steel matrix cermet fuel reported for UO_2 and MOX [20,21] showed a high swelling and matrix rupture when the initial fuel particles were dense. Low-density fuel particles, however, were found to mitigate swelling as their porosity permits the accommodation of fission products accumulated in the irradiation.

The optical micrographs shown in Fig. 5 indicate that all $(Y,Pu,Zr)O_{2-x}$ particles are uniformly distributed in the matrix. This is corroborated by the image analysis and the small HD (4.1 ± 0.2) value obtained.

4. Conclusions

The results presented in this study have demonstrated the feasibility of the fabrication of $(Y,An,Zr)O_{2-x}$ based molybdenum and stainless steel cermets, by a combination of sol–gel, infiltration and conventional blending techniques. The main advantage of this fabrication method is the high flexibility to select the size and volume fraction of the ceramic phase, and the actinide content in the ceramic phase. Materials exhibiting a homogeneous dispersion of the ceramic phase (fuel-bearing phase) have been produced. First tests on fabricating $(Y,Pu,Zr)O_{2-x}$–SS cermet pellets was successful and they are being loaded in fuel pins. Further activities will extend the process to minor actinides incorporated in YSZ particles and dispersed in stainless steel or molybdenum.

Acknowledgements

The authors wish to acknowledge A. Accarier, C. Boshoven, H. Hein, M. Holzhäuser, F. Naisse, R. Voet for their supporting activities in this project.

References

[1] N. Chauvin, R.J.M. Konings, Hj. Matzke, J. Nucl. Mater. 274 (1999) 105.
[2] J. Wallenius, J. Nucl. Mater., EMRT II. doi:10.1016/S0022-3115(03)00181-8.
[3] J. Porta, C. Aillaud, S. Baldi, J. Nucl. Mater. 274 (1999) 174.
[4] K. Bakker, F.C. Klaaseen, R.P.C. Scram, A. Hogenbirk, R. Klein, A. Bos, H. Rakhorst, C.A. Mol, Nucl. Energy, submitted for publication.
[5] V. Troyanov, V. Popov, Iu. Baranev, Prog. Nucl. Energy 38 (2001) 267.
[6] K. Idemitzu, Paul Scherrer Institut Internal Report, TM-43-97-29, 1997, Villigen, Switzerland.
[7] P. Weimar, H. Zimmermann, Internal Report KFK 1893, Kernforschungzentrum Karlsruhe, 1973.
[8] G. Brambilla, P. Gerontopoulos, D. Neri, Energia Nucl. 17 (1979) 217.
[9] A. Fernández, K. Richter, J. Somers, Adv. Sci. Technol. 15 (1999) 167.
[10] K. Richter, A. Fernández, J. Somers, J. Nucl. Mater. 249 (1997) 121.
[11] Institute for Transuranium Elements Annual Report 2000, European Commission, Joint Research Centre, Institute for Transuranium Elements, EUR 19812EN, 2001, p. 115.
[12] A. Fernández, D. Haas, R.J.M. Konings, J. Somers, J. Am. Ceram. Soc. 85 (2002) 694.
[13] Powder diffraction file no. 30-1468, International Centre for Diffraction Data, Newton Square, PA.
[14] QWIN LEICA. Leica Imaging Systems, Cambridge, England 1997.
[15] M.G.H.M. Hendriks, M.J.G.W. Heijman, W.E. van Z, J.E. ten Elshof, H. Verweij, J. Am. Ceram. Soc. 85 (2002) 2097.
[16] Y. Croixmarie, private communication, 2002.
[17] D. White, A.P. Beard, A.H. Willis, Irradiation behavior of dispersion fuels, Internal Report KAPL-P-1849, Knolls Atomic Power Laboratory, Schenectady, NY, 1957.
[18] Y. Croixmarie, E. Abonneau, F. Desmouliere, L. Donnet, A. Fernández, R.J.M. Konings, J. Nucl. Mater., EMRT. doi:10.1016/S0022-3115(03)00162-4.
[19] M.D. Freshley, G.A. Last, Irradiation of magnesium matrix fuel material to high exposures, Internal Report HW-43973, 1956.
[20] B.R.T. Frost, Nuclear Fuel Elements, Pergamon, 1982, p. 247.
[21] J.D.B. Lambert, in: Metallurgical Society Conferences, vol. 42, Gordon and Breach, NY, 1966, p. 137.